JOURNAL OF AGRICULTURAL AND FOOD CHEMISTRY



pubs.acs.org/JAFC
Article

# Selenoprotein K Confers Protection against Iron Dyshomeostasis-Related Neurotoxicity by Regulating the Palmitoylation of TfR-1

Shi-Zheng Jia, Yu Li, Xin-Wen Xu, Yan-Ping Huang, Xiao-Yi Deng, Zhong-Hao Zhang,* and Guo-Li Song*

Cite This: J. Agric. Food Chem. 2025, 73, 12233−12246



**ABSTRACT:** Selenoprotein K (SELENOK), a protein residing in the endoplasmic reticulum (ER), is modulated by dietary selenium and is expressed at elevated levels in neurons. SELENOK has been shown to participate in cellular antioxidant activity and posttranslational palmitoylation. This study presents both in vivo and in vitro evidence that SELENOK deficiency reduces the palmitoylation of TfR-1, thereby impairing transferrin transport and ultimately leading to a decrease in the intracellular iron content, impaired mitochondrial respiratory chain activity and decreased ATP production. Remarkably, restoring SELENOK levels significantly enhanced TfR-1 palmitoylation, increased intracellular iron levels, and restored mitochondrial function, thus ameliorating cognitive deficits in 7 month-old SELENOK knockout mice. Consistent with these findings, iron supplementation also improved mitochondrial function by elevating intracellular iron levels, thereby improving cognitive deficits in 7 month-old SELENOK knockout mice. Therefore, SELENOK exerts its neuroprotective effect by regulating the palmitoylation of TfR-1 to maintain iron homeostasis, thereby protecting mitochondrial function in neurons.

**KEYWORDS:** *SELENOK, TfR-1 palmitoylation, iron, mitochondrial function*

## 1. INTRODUCTION

Mitochondria are indispensable multifunctional organelles for cellular metabolism in almost all eukaryotic cells.[1] Mitochondria primarily function to manufacture ATP via the oxidative phosphorylation (OXPHOS) mechanism, which transforms chemical energy from FADH2 and NADH generated in the citric acid (TCA) cycle into electron flow inside the electron transport chain (ETC).[2] The ETC consists of four multisubunit complexes,[3−6] in addition to a fifth complex, Complex V, which is responsible for converting ADP and inorganic phosphate into ATP.[7] The number of mitochondria reflects the energy demand of a cell, with tissues such as muscles, myocardial cells, and neurons requiring increased mitochondrial content.[8] Mitochondrial dysfunction contributes to various neurodegenerative diseases, as neuronal mitochondria exhibit lower density than other cells, such as muscle cells. Despite this, the brain uses nearly ten times more oxygen and glucose than other tissues.[9,10]

Iron−sulfur (Fe−S) clusters are common cofactors found in many organisms and represent the largest group of metalloproteins. Their primary function is to participate in electron transfer processes. Fe−S clusters play a crucial role in both the TCA cycle and ETC within mitochondria.[11] Numerous Fe−S clusters have been identified in mitochondrial complexes I, II, and III.[12−14] Complex IV functions as a haem aa3-copper oxygen reductase.[15] More than 75% of the iron in the human body is directly utilized in the production of haem or Fe−S cluster cofactors.[16] Therefore, iron content is crucial for the assembly of Fe−S clusters. The intracellular iron concentration is strictly controlled by the iron responsive element−iron regulatory protein (IRE−IRP) system, which involves iron regulatory proteins (IRPs).[17] In iron-deficient cells, IRP binds to iron responsive elements (IREs) on the 3′-untranslated region (UTR) of target mRNAs (such as TfR-1), leading to enhanced stability and transcription. Conversely, IRP binding to the IRE in the 5′-UTR of target mRNAs, including ferritin heavy chain/light-chain (FTH1/FTL), prevents translation.[18,19] Transferrin receptor-1 (TfR-1) facilitates the cellular uptake of iron-bound transferrin (Tf), serving as a major way for cells to obtain iron. Serum Tf can exist in noniron-bound (apo-Tf), monoferric or diferric (holo-Tf) forms.[20] On the cell surface, holo-Tf binds to TfR-1 and enters the cell via endocytosis.[21] In the acidic milieu of the endosome, $Fe^{3+}$ dissociates from Tf, followed by its conversion to $Fe^{2+}$ via metal reductase. Proper functioning of TfR-1 relies on post translational palmitoylation modification while it resides on the cell membrane.

Selenium is a crucial micronutrient that protects against oxidative stress in cells.[22,23] In cases of selenium deficiency, the brain retains more selenium than other tissues.[24] Selenium mostly fulfills its biological purpose by being incorporated into selenoproteins.[25] Selenomethionine improves mitochondrial function by upregulating mitochondrial selenoproteins.[26] Se supplementation effectively inhibits neuronal ferroptosis

Received: September 10, 2024
Revised: April 15, 2025
Accepted: April 24, 2025
Published: April 29, 2025

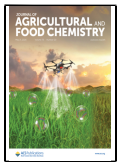





https://doi.org/10.1021/acs.jafc.4c08266
J. Agric. Food Chem. 2025, 73, 12233−12246

through the activation of GPX4 while also inducing an increase in selenoprotein K (SELENOK) expression.[27]

SELENOK, located on the ER membrane and abundantly expressed in the brain, actively participates in regulating both oxidative stress and endoplasmic reticulum stress.[28−30] Additionally, SELENOK modulates the activity of inositol-1,4,5-triphosphate receptor (IP3R), a $Ca^{2+}$ channel protein situated in the ER membrane, through posttranslational palmitoylation.[31] The impaired palmitoylation of TfR-1 has been reported to disrupt iron homeostasis in the brain.[32,33] Given the close relationship between iron homeostasis and oxidative stress and mitochondrial function, it is plausible that SELENOK may be involved in regulating iron homeostasis and mitochondrial function; however, no relevant reports on this topic have been published thus far.

In this study, we observed that knockout/knockdown of SELENOK resulted in a reduction in the palmitoylation of TfR-1, thereby impacting Tf transport and ultimately leading to decreased intracellular iron content, impaired mitochondrial respiratory chain activity, and decreased ATP levels. Notably, these effects were reversed upon the restoration of SELENOK expression or the replenishment of iron.

## 2. MATERIALS AND METHODS

**2.1. Mice.** SELENOK$^{-/-}$ mice developed on the C57BL/6J background were graciously provided by the University of Hawaii. This investigation involved housing C57BL/6J mice and SELENOK$^{-/-}$ mice, aged 4, 7, and 12 months, individually in ventilated cages ($n$ = 3−4) based on their respective group. The living circumstances consisted of a room temperature sustained at 22 ± 2 °C, accompanied by a 12 h alternating light/dark cycle, with unrestricted access to food and water. Body weight assessments were conducted biweekly. At 6 months of age, the diet was switched to either a control or high-iron diet (BIOPIKE M11102). All procedures were conducted in accordance with the instructions sanctioned by the Animal Ethical and Welfare Committee of Shenzhen University (Permit Number: IACUC-202300052).

**2.2. Cell Culture, Treatment, and Adenovirus Transfection.** The culture of N2a and SELENOK$^{-/-}$ N2a cells has been previously described.[30] In brief, the cells were grown in a 1:1 mixture of Opti-MEM and DMEM, supplemented with 6% fetal bovine serum, 100 mg/mL streptomycin, and 100 U/mL penicillin. Primary neuronal cultures were prepared as previously described.[34] The cerebral cortex was dissected from C57BL/6J and SELENOK$^{-/-}$ mouse offspring after birth (P0−P1) and subjected to digestion with 2 mg/mL papain at 37 °C for 30 min. The processed tissue was subsequently triturated by pipetting in DMEM supplemented with 10% FBS. Dissociated cells were cultivated in poly-D-lysine-coated six-well plates at a density of 1 × $10^6$ cells/well for confocal microscopy or at a density of 1 × $10^5$ cells/well. Following a 2 h incubation, the medium was completely substituted with neuron culture medium (50 U/mL penicillin, 0.5 mm L-glutamine and 2% B27), followed by the replacement of half of the culture medium every 2 days.

N2a cells were cultured on a 6-well plate, followed by treatment with the respective drugs for 24 h. The drugs used in this study included artesunate (100 nmol/mL), deferoxamine mesylate (DFOM, 10 μmol/mL), and Dp44 mT (2 μmol/mL). The AAVs used for the overexpression of SELENOK in this research were genetically constructed by OBiO Technology (Shanghai, China). Detailed information can be found as previously described.[35] SELENOK$^{-/-}$ N2a cells were plated in a 6-well plate and allowed to adhere. Then, 750 μL of serum-free culture media combined with virus (virus volume = number of cells × MOI/virus titer; MOI = 200) was introduced to each well and cultured for 2 h. Subsequently, an additional 750 μL of complete culture medium was added. The medium was substituted with new complete culture medium within 24 h. Forty-eight h after transfection, the cells were used for subsequent experiments.

**2.3. Western Blot Analysis.** Brain tissue and cells were subjected to total protein extraction utilizing RIPA buffer, followed by centrifugation at 12,000$g$ for 30 min at 4 °C. The protein concentration was measured using a BCA protein assay kit (Beyotime, Nanjing, China). Protein samples (10−20 μg) were subjected to 10−12% SDS−polyacrylamide gel electrophoresis (SDS−PAGE) and subsequently transferred to 0.45 μm polyvinylidene difluoride membranes (Merck Millipore, Burlington, MA, USA). Then, the membranes were treated overnight at 4 °C with primary antibodies specific for tubulin (Proteintech 66031-1), GAPDH (Proteintech 10494), transferrin (Abcam ab278498), transferrin receptor (TfR-1) (Thermo Fisher 13-6800), FTH1 (Abcam ab75973), IREB2 (Abcam ab181153), and UQCRC2 (Proteintech 14742-1); SDHB (Proteintech 10620-1), MTCO2 (Proteintech 55070-1), and NDUFB8 (Proteintech 14-794-1). Horseradish peroxidase-conjugated secondary antibodies (antirabbit or antimouse, Abcam) were incubated for 1 h at 37 °C. Protein bands were detected using an enhanced chemiluminescence assay kit (Epizyme, Shanghai, China) and visualized using an automated chemiluminescence imaging system (Tanon, Shanghai, People's Republic of China). Band intensity quantification was performed using ImageJ software (National Institutes of Health, Stapleton, New York, USA).

**2.4. Immunofluorescence.** The cultivated cells were fixed with 4% paraformaldehyde (PFA) for 30 min, followed by three washes with PBS, then incubated at room temperature in a solution of 0.5% Triton X-100 and 10% normal goat serum for 30 min. The samples incubated treated with the primary antibody at 4 °C overnight. After washing, the samples were incubated with secondary antibodies in blocking buffer for 1 h. Following another round of washing, the samples were counterstained with DAPI. Imaging analysis was conducted with a Zeiss LSM 880 laser scanning confocal microscope (Carl Zeiss AG, Germany) equipped with z-stack and tile scan capabilities.

**2.5. Tf Internalization.** Live cell imaging was employed to assess the internalization of Tf. After incubation with Alexa 561−Tf (25 μg/mL) at 37 °C for 5 min, Tf internalization was quantified. Imaging analysis was performed using a SIM superresolution microscope (TI2-N-SIM-S) or an OLYMPUS (APX-1000) microscope.

**2.6. Palmitoylated Proteins Profiling.** Palmitoylated proteins were enriched using the acyl-ABE assay with protocol optimization.[36] Briefly, protein lysates (1 mg) were alkylated with 50 mM N-ethylmaleimide in protease inhibitors overnight at 4 °C. Following triple chloroform−methanol (CM) precipitation, samples were bifurcated and subjected to hydroxylamine (+HA) and without hydroxylamine (−HA). The + HA sample (200 μL) was treated with 800 μL of Solution A which consisted of 700 μL of 1 M HA in PBS, 20 μL of 10% Triton X-100, 10 μL of protease inhibitor, 250 μL of 4 mM HPDP-biotin (A8008; APExBIO) and 20 μL of PBS. Conversely, the -HA sample (200 μL) was incubated with 800 μL of Solution B, comprising 670 μL of PBS, 20 μL of 10% Triton X-100, 10 μL of protease inhibitor, 250 μL of 4 mM HPDP-biotin and 50 μL of 1 M Tris−HCl (pH 7.4) at 25 °C for 2 h. After CM precipitation, the samples were reconstituted in 50 μL of TB buffer and mixed with 0.9 mL of LB buffer (containing protease inhibitors) and 20 μL streptavidin-agarose (20353; Thermo Fisher Scientific) at 25 °C for 3 h. The precipitates were eluted in 50 μL LB containing 1% β-mercaptoethanol, denatured at 100 °C for 8 min and stored at −20 °C.

**2.7. Isolation and Detection of Membrane Proteins.** Cells were inoculated on a 6-well plate at the density of 5 × $10^5$ cells per well and washed three times with PBS. Subsequently, 400 μL of Sulfo−NHS−SS-Biotin was added to each well, followed by a 30 min incubation at 4 °C. Afterward, the wells were rinsed three times with precooled 50 mM glycine and soaked for 5 min each time. Then, 60 μL of IP buffer (precooled PBS containing 1% Triton X-100 and protease inhibitor) was introduced into each well, followed by a 10 min incubation on ice and centrifugation at 14,000 rpm for 10 min at 4 °C; 10 μL of the supernatant was collected as input, while the


https://doi.org/10.1021/acs.jafc.4c08266
J. Agric. Food Chem. 2025, 73, 12233−12246

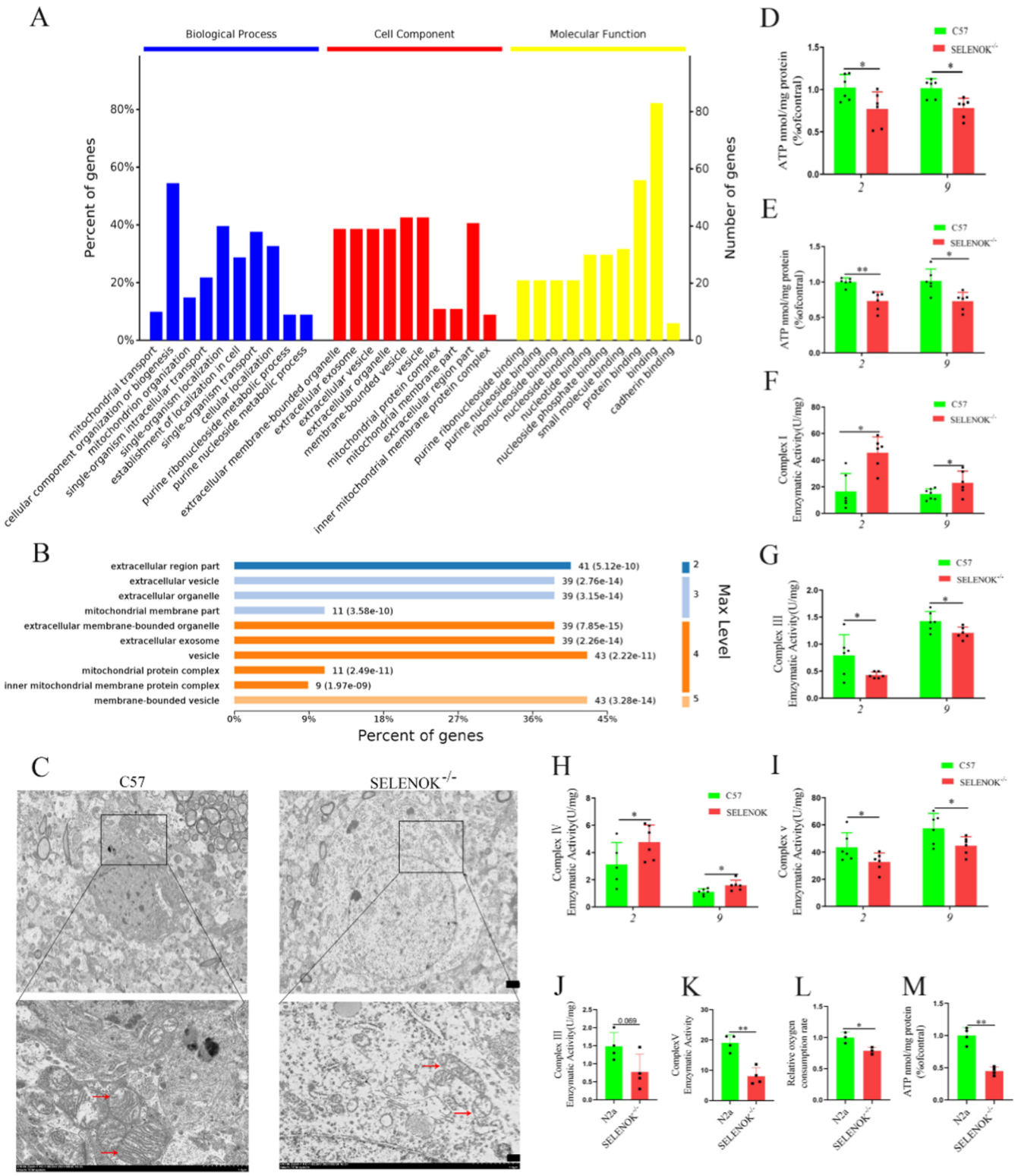


**Figure 1.** SELENOK deficiency affects mitochondrial function in vitro and in vivo. (A,B) Proteomic analysis of the hippocampi of 7 month-old SELENOK$^{-/-}$ mice. (C) The morphology of mitochondria in hippocampal neurons observed by electron microscopy. Scale bars, 10 $\mu$m (upper panel) and 2 $\mu$m (lower panel). (D,E) Mitochondrial ATP content in 7 month-old cortex (D) and hippocampal (E) brain homogenates ($n$ = 6). (F−I) Activity of the mitochondrial respiratory chain complex in the cortex of 2 month-old and 9 month-old mice. (F) Mitochondrial complex I (*$p$ < 0.05, $n$ = 6, 9 month-old C57, $n$ = 7). (G) Mitochondrial complex III (*$p$ < 0.05, $n$ = 6). (H) Mitochondrial complex IV (*$p$ < 0.05, $n$ = 6, 2 month-old C57, $n$ = 5). (I) Mitochondrial complex V (*$p$ < 0.05, $n$ = 6). (J,K) Activity of the mitochondrial respiratory chain complex in WT and SELENOK$^{-/-}$ N2a cells (**$p$ < 0.01, $n$ = 4). (L) The relative Oxygen consumption rate (OCR) in WT and SELENOK$^{-/-}$ N2a cells (*$p$ < 0.01, $n$ = 3). (M) Mitochondrial ATP content in WT and SELENOK$^{-/-}$ N2a cells (**$p$ < 0.01, $n$ = 4).


https://doi.org/10.1021/acs.jafc.4c08266
J. Agric. Food Chem. 2025, 73, 12233−12246

residual supernatant was incubated with 50 and 5 μL of streptavidin agarose at 4 °C for 2 h. After being washed 5 times with detergent (precooled PBS containing 1% Triton X-100), the samples were centrifuged at 5000 rpm for 1 min at 4 °C. Finally, the precipitates were eluted in 30 μL of 6× loading buffer and incubated at 65 °C for 10 min, after which the supernatant was collected for WB analysis.

**2.8. Intracellular $Fe^{2+}$ Levels.** The intracellular $Fe^{2+}$ levels in SELENOK-KO N2a cells and SELENOK-KD neurons were measured using a multiwavelength microplate reader after labeling with ferroOrange, which exhibits enhanced fluorescence upon binding to free $Fe^{2+}$. The cultured SELENOK-KO N2a and SELENOK-KD neuronal cells were treated with 1 μM ferroOrange (DOJINDO, F374) for 30 min at 37 °C, followed by immediate analysis using a microplate reader with an excitation wavelength of 543 nm.

**2.9. Mitochondrial Content.** The intracellular mitochondrial fluorescence levels in SELENOK-KO N2a cells and SELENOK-KD neurons were measured using a multiwavelength microplate reader after labeling with MitoBright LT Red, which exhibits enhanced fluorescence upon binding to mitochondria. The cultured SELENOK-KO N2a and SELENOK-KD neuronal cells were incubated with 0.1 μM MitoBright LT Red working solution (DOJINDO, MT11) for 30 min at 37 °C, followed by immediate analysis using a microplate reader with an excitation wavelength of 561 nm.

**2.10. Mitochondrial Respiratory Chain Complex Activity.** The activity of the mitochondrial respiratory chain complexes was assessed following the instructions provided with the respective reagents. Mitochondrial complex I (Solarbio, BC0515), mitochondrial complex III (Solarbio, BC3245), mitochondrial complex IV (Solarbio, BC0945), and mitochondrial complex V (Solarbio, BC1445) were obtained.

**2.11. Morris Water Maze Test.** The Morris water maze is a well-established test for evaluating the spatial learning and memory abilities of mice. The experimental procedure of the Morris water maze test consists of two stages: an initial 5 day period of positioning and navigation, during which the mice are placed facing the wall in various quadrants of a pool. Once the mouse of interest located the platform, the recording time ceased. If the mouse failed to find and mount the platform within 60 s, that mouse was guided to board the platform and allowed to adapt for approximately 10 s. After 5 days of training, the platform was removed for subsequent spatial exploration experiments, which measured both the duration that the mice spent in the original platform quadrant and their frequency of passing through the original platform position after 24 and 72 h.

**2.12. Y-Maze Test.** The Y-maze test is a behavioral test that capitalizes upon animals' innate curiosity to explore, and spontaneous alternation behavior in this test is considered an indicator of short-term spatial working memory. The Y-maze apparatus consists of three opaque plastic arms (designated I, II, III) with an angular separation of 120° between two adjacent arms. The mouse was gently placed at the center point of the maze and allowed to explore freely for 3 min. Subsequently, the sequence in which the mice entered each arm was recorded and analyzed.

**2.13. Elevated Plus Maze.** The elevated plus maze test is a behavioral assay that capitalizes on innate exploratory curiosity and conflicting behaviors related to fear of the open arms of animals: the number of times the animals entered the open arms and the duration spent in the open arms were considered indicators of anxiety in this test. The mouse was gently placed at the center of the maze and allowed to explore freely for 3 min. Finally, both the number of times the mice entered the open arms and the time spent in the open arms were recorded and analyzed.

**2.14. Oxygen Consumption Rate.** Oxygen consumption Rate was quantified utilizing the Extracellular Oxygen Consumption Rate Assay Kit (Elabscience, E-BC-F068) in accordance with the manufacturer's guidelines.

**2.15. Statistical Analysis.** GraphPad Prism 9 (GraphPad Software, La Jolla, CA, USA) was utilized to analyze the data, which were presented as the means ± SD (*$p$ < 0.05, **$p$ < 0.01, ***$p$ < 0.001, ****$p$ < 0.0001). Experimental comparisons were conducted utilizing ANOVA, succeeded by the relevant post hoc test (Dunnett), or employing an unpaired Student's $t$-test. The statistical methods employed for each quantitated data, together with the corresponding sample sizes, are detailed in the pertinent figure legends.

## 3. RESULTS

**3.1. SELENOK Deficiency Impairs Mitochondrial Function.** To validate the impact of SELENOK on the brain function, SELENOK$^{-/-}$ mice and cells were generated using the CRISPR-Cas9 system.[30] SELENOK expression levels were quantified by Western blot and a very low level of SELENOK expression was observed in SELENOK$^{-/-}$ N2a cells and in SELENOK$^{-/-}$ mice (Figure S1A,B). Proteomic analysis of the hippocampi of 7 month-old SELENOK$^{-/-}$ mice revealed a close association between SELENOK and mitochondrial function (Figure 1A,B). The electron microscopy results confirmed that SELENOK deficiency led to altered mitochondrial morphology in neurons, characterized by decreased mitochondrial volume and loss of mitochondrial cristae (Figure 1C). The major role that mitochondria play in cells is to produce ATP through mitochondrial respiratory chain complexes. Therefore, we detected ATP levels in 2- and 9 month-old SELENOK$^{-/-}$ mice. The results showed ATP levels were significantly decreased in both cortical and hippocampal regions (Figure 1D,E). Additionally, we observed that the activities of complexes I and IV were significantly increased, while those of complexes III and V were significantly reduced in the cortical regions of 2- and 9 month-old SELENOK$^{-/-}$ mice (Figure 1F−I). Consistent with these findings, SELENOK$^{-/-}$ N2a cells exhibited significantly reduced complex V activity, OCR and ATP levels compared to wild-type N2a cells (Figure 1J−M). Mitochondrial function assessment also revealed a significant decrease in mitochondrial content and cell viability in SELENOK-knockdown neurons (Figure S4C−F). These findings collectively suggest that SELENOK expression is crucial for maintaining mitochondrial homeostasis.

**3.2. SELENOK Deficiency Reduces Iron−Sulfur Cluster Protein Levels.** Fe−S clusters serve as essential cofactors, primarily facilitating electron transfer in the mitochondrial respiratory chain. Therefore, we detected the expression levels of the key subunit proteins NDUFB8, SDHB, UQCRC2 and MTCO2 in the mitochondrial complexes. Notably, a significant reduction in UQCRC2 expression was observed in the cortex and hippocampus of 7- and 12 month-old SELENOK$^{-/-}$ mice (Figures 2A−D and S2E−G). In addition, SELENOK$^{-/-}$ N2a cells (Figure 2E,F) and SELENOK-knockdown primary neurons (Figure 2G,H) exhibited significantly decreased levels of NDUFB8, SDHB, UQCRC2, and MTCO2. Our results confirmed that SELENOK deficiency impairs iron−sulfur [Fe−S] cluster/haem biogenesis.

**3.3. SELENOK Deficiency Reduces the Intracellular Iron Content.** The assembly of iron−sulfur clusters is closely associated with iron content; treatment with the iron chelating agents DFOM or Dp44 mT significantly reduced both iron content and iron−sulfur protein expression in vitro (Figure S3A−F). Therefore, we detected changes in iron content after knockout of the SELENOK gene. In SELENOK$^{-/-}$ N2a cells, total iron content was significantly reduced (Figure 3A). Iron exists in two interconvertible forms: ferric ($Fe^{3+}$) and ferrous ($Fe^{2+}$). Therefore, we detected $Fe^{2+}$ levels in SELENOK$^{-/-}$ N2a cells and found a significant decrease (Figure 3B).


https://doi.org/10.1021/acs.jafc.4c08266
J. Agric. Food Chem. 2025, 73, 12233−12246

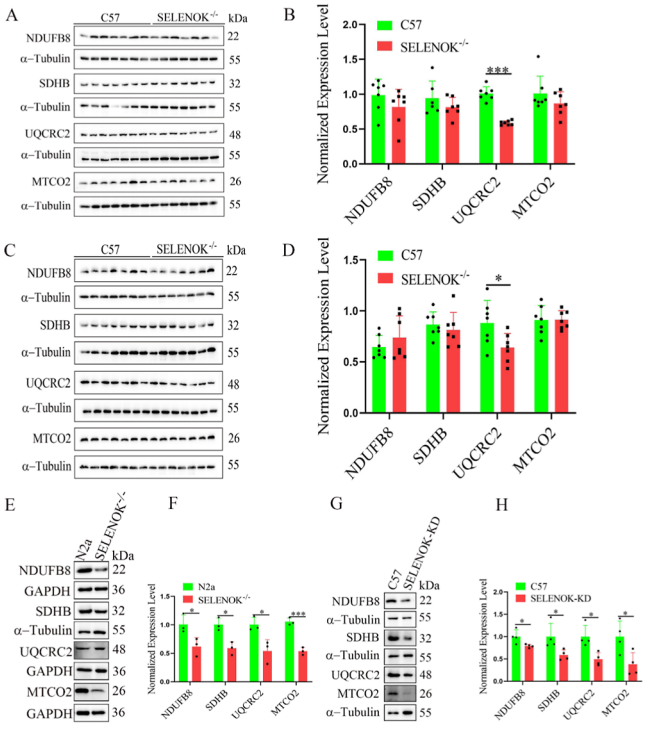


**Figure 2.** SELENOK deficiency reduces iron−sulfur cluster protein expression in vitro and in vivo. (A−D) Representative immunoblot analysis of NDUFB8, SDHB, UQCRC2, and MTCO2 in 7 month-old cortical (A,B) and hippocampal (C,D) brain homogenates (*$p < 0.05$, $n = 7$). (E,F) Immunoblot analysis of NDUFB8, SDHB, UQCRC2, and MTCO2 in WT and SELENOK$^{-/-}$ N2a cells ($n = 3$). (G,H) Immunoblot analysis of NDUFB8, SDHB, UQCRC2, and MTCO2 in WT and SELENOK-knockdown nerve cells (*$p < 0.05$, $n = 4$).

Moreover, total iron, $Fe^{2+}$, and $Fe^{3+}$ contents were significantly reduced in the cortical regions of 12 month-old SELENOK$^{-/-}$ mice (Figure 3C−E). To corroborate these findings, ICP−MS was utilized to measure the iron concentration in the cortex of 7 and 12 month-old SELENOK$^{-/-}$ mice, revealing a notable decrease in iron levels (Figure 3F). Since most cellular iron is transported into mitochondria for haem and Fe/S cluster biogenesis,[37,38] we assessed both the mitochondrial and cytoplasmic iron content. The results demonstrated a significant reduction in both the mitochondrial and cytoplasmic iron content in cortical brain homogenates from 7- and 12 month-old SELENOK$^{-/-}$ mice (Figure 3G,H). All of the above results confirm that SELENOK gene knockout leads to decreased overall cellular iron levels.

Transferrin receptors (TfR) play a crucial role in facilitating the cellular uptake of transferrin-bound ferric ions, serving as the primary mechanism by which cells acquire extracellular iron.[39] Excess intracellular iron is sequestered into ferritin for storage, and this polymeric protein consists of two subunits, H-ferritin and L-ferritin. Cellular iron homeostasis is post-transcriptionally regulated by IRPs.[40] Therefore, we assessed the expression levels of those proteins involved in iron homeostasis. The levels of IREB2, Tf, and TfR-1 significantly increased in both cortical and hippocampal regions in 7 month-old SELENOK$^{-/-}$ mice. Additionally, there was a significant reduction in FTH1 levels in both regions (Figure 3I,J). Similar results were observed in primary neurons with SELENOK knockdown: the levels of IREB2 and TfR-1 were significantly increased, while the level of FTH1 was significantly decreased (Figure 3K,L).

**3.4. SELENOK Deficiency Reduces TfR-1 Palmitoylation and Impairs Transferrin Endocytosis.** The transferrin receptor (TfR-1), which is responsible for facilitating cellular iron uptake and regulating iron homeostasis, undergoes posttranslational palmitoylation. SELENOK acts as a chaperone of DHHC6 and plays a crucial role in various protein palmitoylation processes.[41] Therefore, we detected the palmitoylation levels of TfR-1 in SELENOK$^{-/-}$ mice and SELENOK$^{-/-}$ N2a cells. Our results showed significantly reduced TfR-1 palmitoylation within the cortical areas of 7 month-old SELENOK$^{-/-}$ mice and SELENOK$^{-/-}$ N2a cells (Figure 4A,B). Additionally, the expression level of TfR-1 on the cell membrane was significantly decreased (Figure 4C,D). A notable reduction in the Tf transport rate was also detected in SELENOK$^{-/-}$ N2a cells (Figure 4E,F). Furthermore, both the Tf transport rate and the $Fe^{2+}$ concentration was significantly reduced in SELENOK-knockdown neurons (Figure S4A,B).

**3.5. Restoring Expression of SELENOK/Artesunate Treatment Enhances Mitochondrial Function.** SELENOK$^{-/-}$ N2a cells were cultured with artesunate (100 nM) (a TfR-1 palmitoylation enhancer) for 24 h or subjected to SELENOK restoration (SELENOK-RE). Then, the palmitoylation of TfR-1 and mitochondrial function were assessed. Our findings demonstrated that both artesunate treatment and SELENOK-RE significantly enhanced TfR-1 palmitoylation and cell membrane expression (Figure 5A−D). Moreover, there was a significant increase in the rate of Tf transport and $Fe^{2+}$ content (Figure 5E−G). Additionally, FTH1 levels were considerably higher in both SELENOK-RE N2a cells and those treated with artesunate (Figure S5B,C). Furthermore, the levels of NDUFB8, SDHB, UQCRC2 and MTCO2 were significantly increased in SELENOK-RE N2a cells (Figure 5H). Importantly, mitochondrial content, ATP content, and cell viability were significantly improved in SELENOK-RE N2a cells (Figure 5I−K). These results confirm that SELENOK restoration improves mitochondrial function by increasing the palmitoylation level of TfR-1, thereby increasing the iron content.

**3.6. Restoring the Expression of SELENOK Enhances Mitochondrial Function and Cognitive Function in Mice.** SELENOK levels were found to be significantly higher in the hippocampal regions of 7 month-old SELENOK$^{-/-}$-RE mice (Figure S5D), in contrast to the significantly reduced levels of IREB2 and TfR-1. Additionally, there was a significant increase in FTH1 levels in the hippocampal regions of 7 month-old SELENOK$^{-/-}$-RE mice (Figure 6A). Restoration of SELENOK expression also led to a significant increase in UQCRC2 expression in the hippocampus of 7 month-old SELENOK$^{-/-}$-RE mice (Figure 6B). Electron microscopy confirmed that restoring SELENOK expression reversed the morphological changes in mitochondria caused by SELENOK knockout, as indicated by an increase in the number of mitochondrial cristae (Figure 6C). Furthermore, restoring the expression of SELENOK increased the ATP content within the hippocampus (Figure 6D). Spatial learning ability was assessed by measuring escape latency, i.e., the time taken for mice to locate hidden platforms in the Morris water maze test. As depicted in Figure 6E, the escape latency did not vary significantly between the groups of mice. However, the SELENOK$^{-/-}$-RE mice spent a significantly greater amount


https://doi.org/10.1021/acs.jafc.4c08266
J. Agric. Food Chem. 2025, 73, 12233−12246

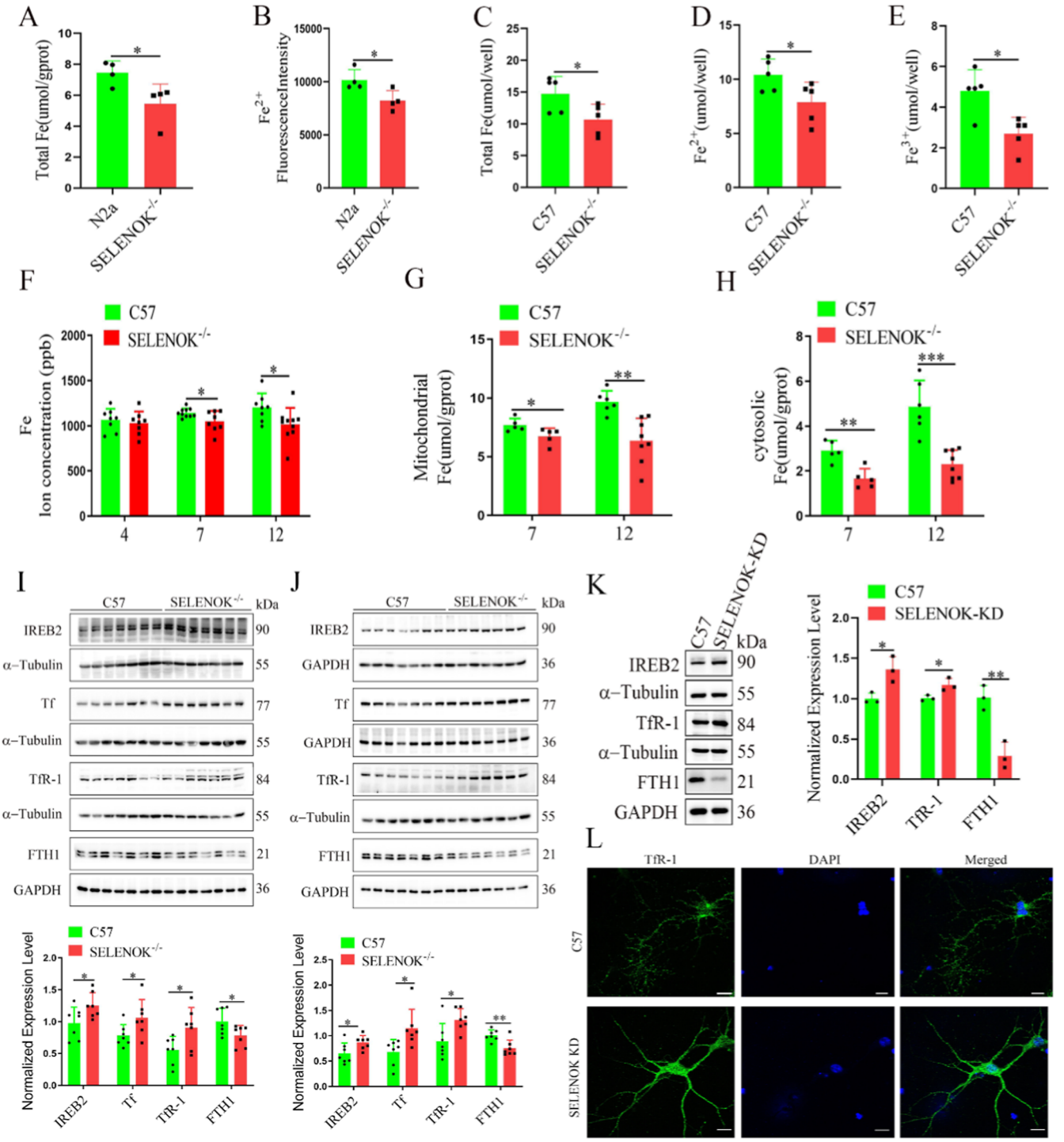


**Figure 3.** SELENOK deficiency reduces the intracellular iron content in vitro and in vivo. (A,B) Total iron and $Fe^{2+}$ content in SELENOK$^{-/-}$ N2a cells ($n$ = 4). (C–E) Total iron, $Fe^{2+}$, and $Fe^{3+}$ content in 12 month-old brain cortex homogenates (*$p$ < 0.05, $n$ = 5). (F) ICP–MS analysis of the iron content in the cortex of mice. (G,H) Mitochondrial and cytosolic iron content in 7 and 12 month-old brain cortex homogenates. (I,J) Representative immunoblot analysis of IREB2, Tf, TfR-1, and FTH1 in 7 month-old cortical (I) and hippocampal (J) brain homogenates (*$p$ < 0.05, $n$ = 7). (K) Representative immunoblot analysis of IREB2, TfR-1, and FTH1 in WT and SELENOK-knockdown primary neurons ($n$ = 3). (L) Immunofluorescence images of TfR-1 in WT and SELENOK-knockdown primary neurons (scale bar: 10 $\mu$m).

of time in the original platform quadrant than the SELENOK$^{-/-}$ control group during the probe trial at 24 and 72 h (Figure 6G,I). Moreover, the SELENOK$^{-/-}$-RE group exhibited a significantly greater number of platform crossings over the original platform location in the 72 h probe experiment (Figure 6H). In the Y-maze test, restoring SELENOK expression significantly increased the spontaneous alternation rate of the mice (Figure 6K). Moreover, compared to SELENOK$^{-/-}$ mice, SELENOK$^{-/-}$-RE mice showed a significant increase in open arm entries and time spent in the open arms in the elevated plus maze test (Figure 6L,M).

**3.7. Iron Supplementation Reverses the Mitochondrial Dysfunction Caused by SELENOK Deficiency.** Iron supplementation also significantly increased the protein


https://doi.org/10.1021/acs.jafc.4c08266
J. Agric. Food Chem. 2025, 73, 12233–12246

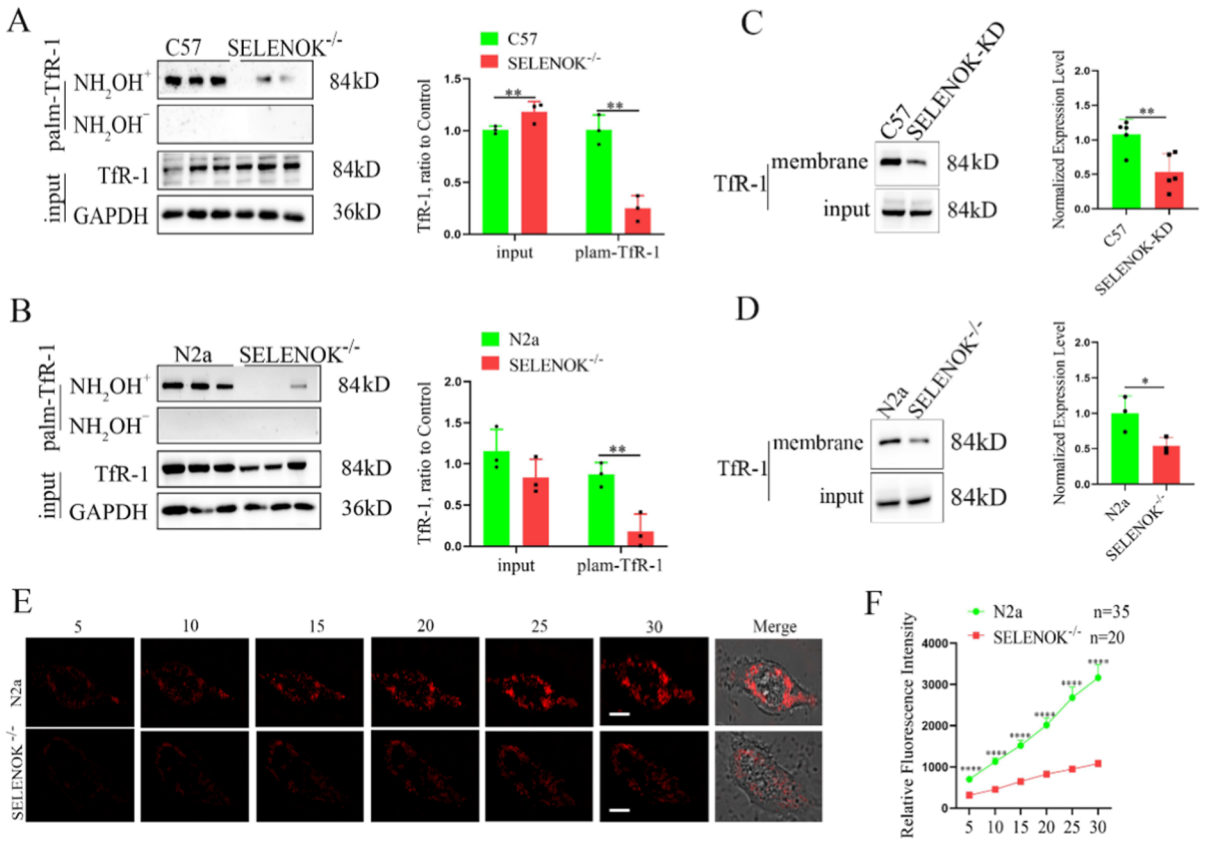


**Figure 4.** SELENOK deficiency leads to decreased palmitoylation, reduced accumulation of TfR-1 on the plasma membrane, and reduced endocytosis of transferrin. (A) Representative immunoblots and measurement of TfR-1 protein expression and palmitoylation levels in cortical lysates from 7 month-old wild-type (C57) and SELENOK$^{-/-}$ mice. Acyl-ABE was found to be enriched in palmitoylated proteins (**$p < 0.01$, $n = 3$). (B) Immunoblots and quantification of TfR-1 protein expression and palmitoylation levels in wild-type (N2a) and SELENOK$^{-/-}$ N2a cells ($n = 3$). (C) Immunoblots and quantification of TfR-1 protein expression in the cell membrane of SELENOK-knockdown neurons (*$p < 0.05$, $n = 5$). (D) Immunoblots and quantification of TfR-1 protein expression in the cell membrane of wild-type (N2a) and SELENOK$^{-/-}$ N2a cells ($n = 3$). (E,F) Relative mean fluorescence intensity of the Alexa 561−Tf signal after 30 min in wild-type (N2a) and SELENOK$^{-/-}$ N2a cells; $n \geq 3$ experiments were performed (scale bar: 10 $\mu$m). (****$p < 0.0001$, N2a cells, $n = 35$; SELENOK$^{-/-}$ cells, $n = 20$).

expression levels of FTH1 (Figure S6A,B) and UQCRC2 (Figure 7A,B) in both the cortex and hippocampus of 7 month-old SELENOK$^{-/-}$ mice, as well as the FTH1 expression level in SELENOK$^{-/-}$ N2a cells (Figure S6C). Furthermore, cell activity initially increased with iron content but subsequently decreased at higher concentrations in SELENOK$^{-/-}$ N2a cells (Figure 7C). Additionally, iron treatment significantly upregulated the protein expression levels of NDUFB8, SDHB, UQCRC2, and MTCO2 in SELENOK$^{-/-}$ N2a cells (Figure 7D). The results of electron microscopy also confirmed that iron treatment reversed the mitochondrial morphological changes caused by SELENOK knockout (Figure 7E). Moreover, iron treatment significantly increased the ATP content (Figure 7F). Even though there were no notable differences in escape latency among the various groups of mice (Figure 7G), during the 24 and 72 h probe trial, iron-supplemented mice spent a significantly longer duration in the original platform quadrant than did the mice in the SELENOK$^{-/-}$ control group (Figure 7I,K). In the Y-maze test, iron treatment significantly increased spontaneous alternation (Figure 7M). Moreover, iron supplementation led to a significant increase in the number of open-arm entries and time spent in the open arms in the elevated plus maze test compared with those of the SELENOK$^{-/-}$ mice (Figure 7N,O).

## 4. DISCUSSION

Selenium plays a key role as a trace element in ensuring the brain functions normally. However, iron accumulation in mouse brain tissue has been linked to excessive Na2SeO3 supplementation.[42] Furthermore, a diet lacking selenium has been reported to significantly raise the levels of transferrin and transferrin receptor mRNA expression in rat liver.[43] These findings suggest a possible role for selenium in modulating iron metabolism. Although most research currently focuses on the antioxidant function of selenium, particularly its involvement in ferroptosis regulation through the activity of the selenium-containing enzyme GPX4.,[27,44] the precise regulatory mechanism between selenium and iron homeostasis remains unclear. Notably, selenium supplementation effectively inhibited neuronal ferroptosis triggered by excessive iron while simultaneously increasing SELENOK expression levels,[27] indicating the possible involvement of SELENOK in the regulation of iron homeostasis. This study revealed that SELENOK plays a crucial role in coordinating brain iron homeostasis and mitochondrial function and discovered a new mechanism by which SELENOK regulates iron homeostasis.

Emerging research suggests that disrupted iron homeostasis and mitochondrial dysfunction are key factors in various neurodegenerative diseases.[45,46] Our previous study demonstrated that SELENOK knockout leads to elevated intracellular


https://doi.org/10.1021/acs.jafc.4c08266
J. Agric. Food Chem. 2025, 73, 12233−12246

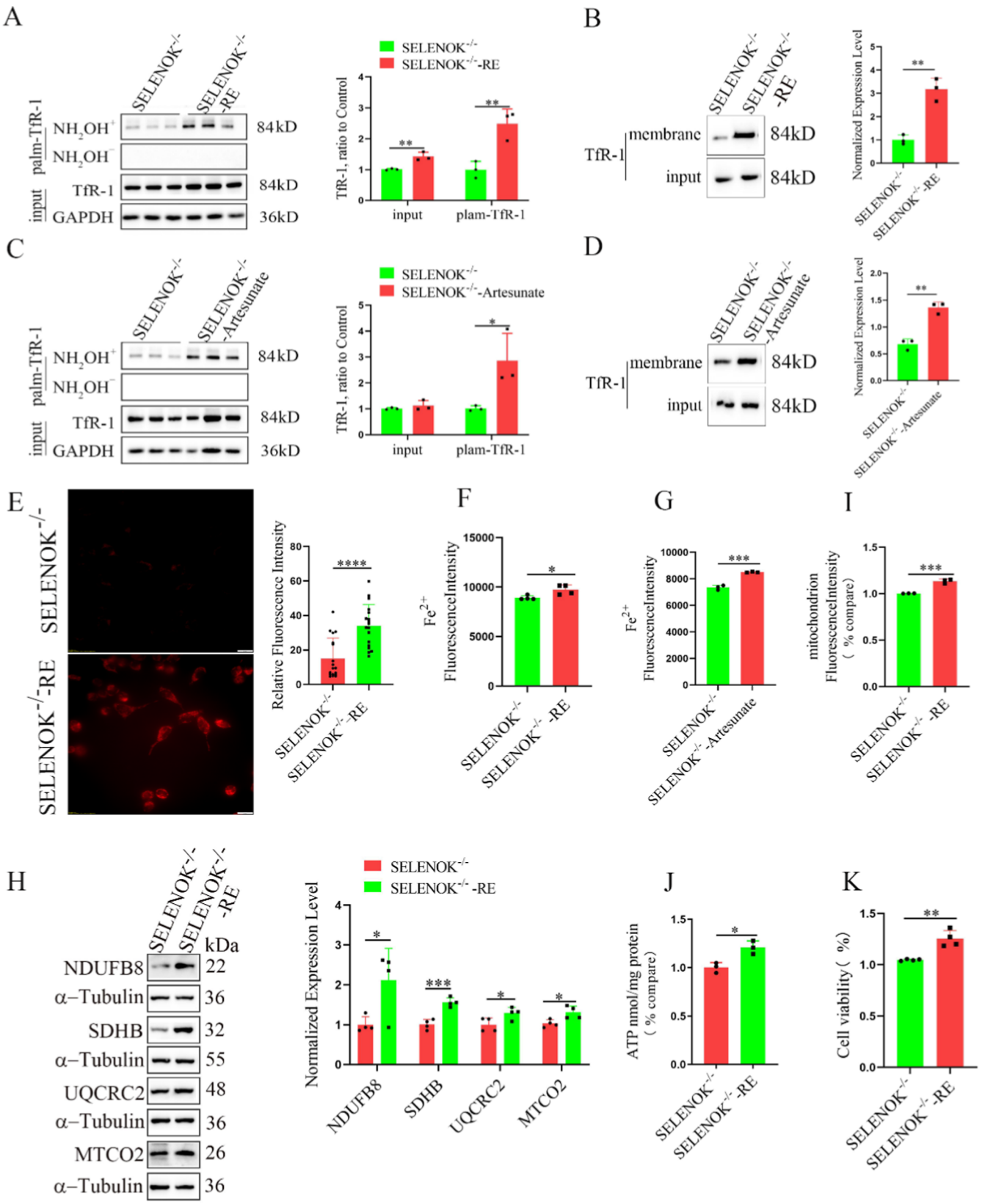


**Figure 5.** Restoring SELENOK expression increases iron content and improves mitochondrial function. (A,B) Levels of TfR-1 palmitoylation (A) and cell membrane expression levels (B) in SELENOK-RE cells. (C,D) Levels of TfR-1 palmitoylation (C) and cell membrane expression (D) in SELENOK$^{-/-}$ cells treated with 100 nM artesunate for 24 h. (E) Relative mean fluorescence intensity of the Alexa 561−Tf signal after 15 min in SELENOK-RE cells; $n$ = 3 (scale bar: 20 $\mu$m) (cells $n$ = 18). (F) $Fe^{2+}$ content in SELENOK-RE cells (*$p$ < 0.05, $n$ = 4). (G) $Fe^{2+}$ content in SELENOK cells treated with 100 nM artesunate (*$p$ < 0.05, $n$ = 3). (H) Immunoblot analysis of NDUFB8, SDHB, UQCRC2, and MTCO2 in SELENOK-RE N2a cells. (I) Mitochondrial content in SELENOK-RE N2a cells (***$p$ < 0.001, $n$ = 3). (J) ATP content in SELENOK-RE cells (*$p$ < 0.05, $n$ = 3). (K) Viability of SELENOK-RE N2a cells (**$p$ < 0.01, $n$ = 4).



https://doi.org/10.1021/acs.jafc.4c08266
J. Agric. Food Chem. 2025, 73, 12233−12246

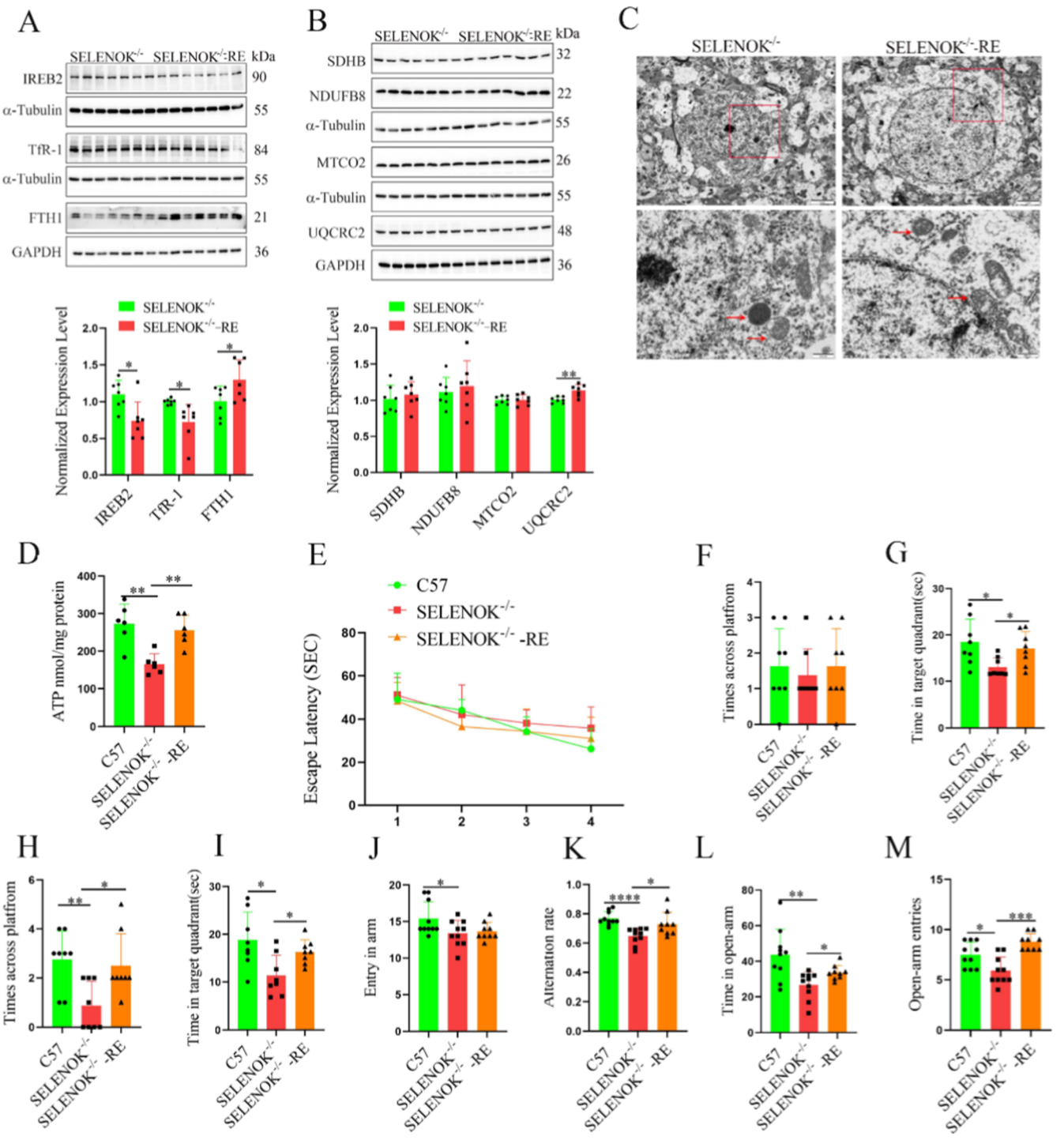


**Figure 6.** Restoring the expression of SELENOK enhances mitochondrial function in vivo. (A) Representative immunoblot analysis of IREB2, TfR-1, and FTH1 in 7 month-old SELENOK$^{-/-}$-RE mouse hippocampal brain homogenates (*$p$ < 0.05, $n$ = 7). (B) Immunoblot analysis of NDUFB8, SDHB, UQCRC2, and MTCO2 in 7 month-old SELENOK$^{-/-}$-RE mouse hippocampal brain homogenates (**$p$ < 0.01, $n$ = 7). (C) Electron micrographs showing mitochondria in hippocampal neurons. Scale bars, 2 $\mu$m (upper panel) and 500 nm (lower panel). (D) ATP content in 7 month-old SELENOK$^{-/-}$-RE mice (**$p$ < 0.01, $n$ = 6). (E) In the hidden platform test, the mice were tested for 4 days, and the escape latency of each mouse was recorded. (F−I) In the 24 h (F,G) and 72 h (H−I) probe trials, the time required for the mouse to swim in the target quadrant where the hidden platform was previously placed and the number of times the mouse crossed the position of the platform were recorded. A total of 8 mice were tested per group. (J,K) The frequency of mouse entry into each arm was recorded, and the alternation rate was calculated in the Y-maze test. (L,M) For the elevated plus maze test, the number of times the mice entered the open arms and the time spent in the open arms are shown. C57, SELENOK$^{-/-}$ $n$ = 10, SELENOK$^{-/-}$-RE $n$ = 9.

ROS levels in N2a cells.[47] Proteomic analysis of the hippocampus of 7 month-old SELENOK$^{-/-}$ mice revealed a close association between SELENOK and mitochondrial function. Mitochondria primarily generate ATP through the respiratory chain while concomitantly producing reactive oxygen species,[48] thus rendering them highly susceptible to


https://doi.org/10.1021/acs.jafc.4c08266
J. Agric. Food Chem. 2025, 73, 12233−12246

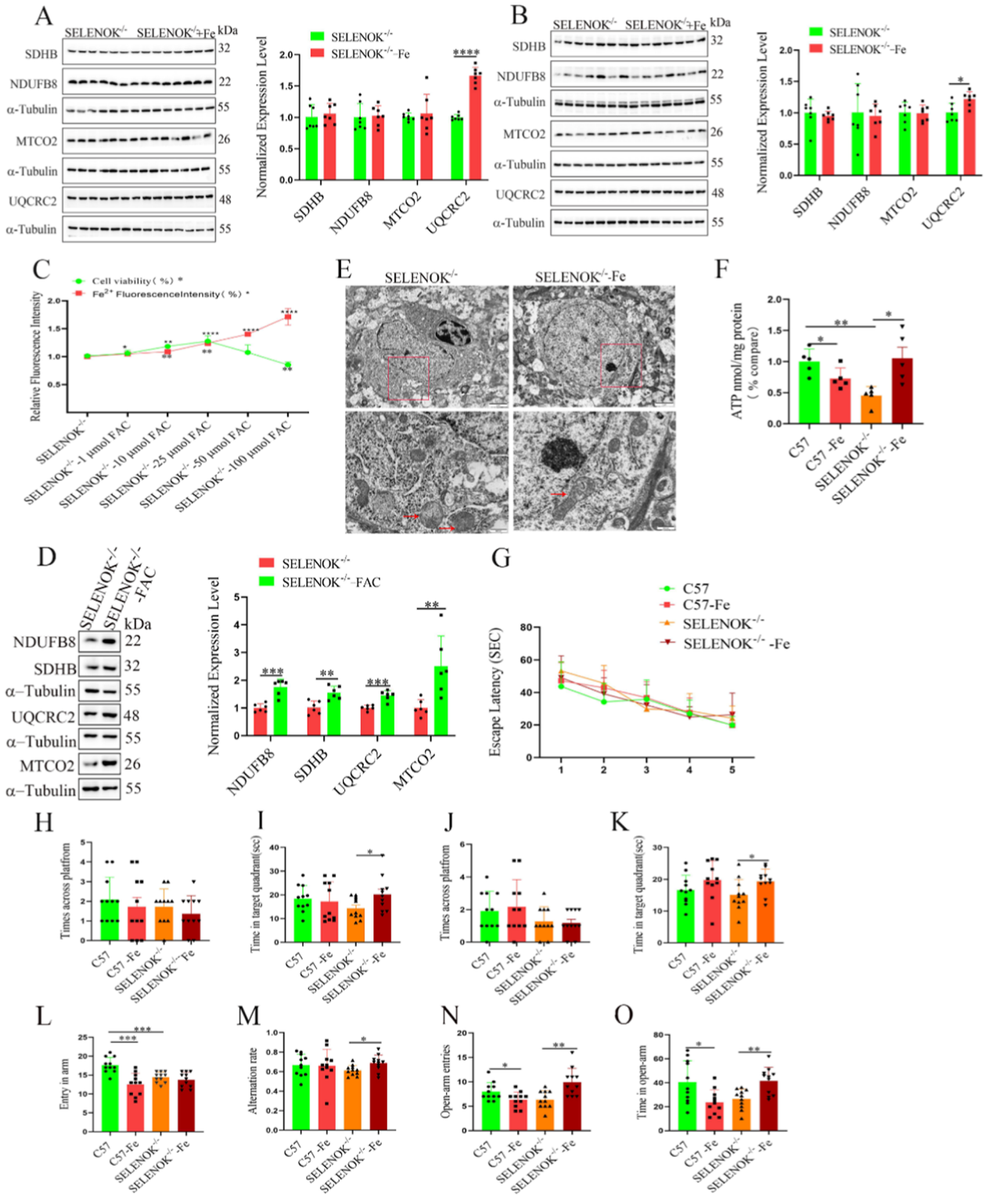


**Figure 7.** Reversal of SELENOK knockout-induced mitochondrial dysfunction by iron supplementation in vitro and in vivo. (A,B) Representative immunoblot analysis of NDUFB8, SDHB, UQCRC2, and MTCO2 in cortex (A) and hippocampal (B) brain homogenates from 7 month-old iron-supplemented mice (*$p < 0.05$, $n = 7$). (C) $Fe^{2+}$ concentration and cell viability of SELENOK$^{-/-}$ cells ($n = 4$). (D) Representative immunoblot analysis of NDUFB8, SDHB, UQCRC2, and MTCO2 in SELENOK$^{-/-}$ N2a cells ($n = 6$). (E) Electron micrographs showing mitochondria in hippocampal neurons. Scale bars, 2 $\mu$m (upper panel) and 500 nm (lower panel). (F) ATP content in 7 month-old iron-supplemented mice (*$p <$ 0.05, $n = 5$). (G) In the hidden platform test, the mice were tested for 5 days, and the escape latency of each mouse was recorded. (H−K) In the 24 h (H,I) and 72 h (J,K) probe trials, the time that the mouse swam in the target quadrant where the hidden platform was previously placed and the number of times the mouse crossed the position of the platform were recorded. (L,M) The frequency of mouse entry into each arm was recorded, and the alternation rate was calculated in the Y-maze test. (N,O) The data illustrated the number of times the mice accessed the open arms and the amount of time they remained there in the elevated plus maze test. A total of 11 mice were tested per group.



https://doi.org/10.1021/acs.jafc.4c08266
J. Agric. Food Chem. 2025, 73, 12233−12246

oxidative damage. Our results revealed that knockout of SELENOK significantly upregulated the activity of mitochondrial complexes I and IV while downregulating the activity of complexes III and V and ATP levels. Additionally, transmission electron microscopy was used to assess morphological changes associated with mitochondrial damage, and the results confirmed that loss of SELENOK led to aberrant mitochondrial morphology in neurons. Collectively, these findings highlight that loss of SELENOK disrupts mitochondrial homeostasis in neurons.

Fe−S clusters play vital roles as cofactors, mainly by assisting electron transfer in the mitochondrial respiratory chain. In this process, through complexes I, II, and III, Fe−S clusters move electrons to cytochrome c, which is accompanied by the creation of mitochondrial ROS.[11] SELENOK deficiency causes a drop in both the expression level and activity of the mitochondrial respiratory complex III [Fe−S] cluster subunit UQCRC2 (CIII) in SELENOK$^{-/-}$ mice. Our findings also demonstrated significantly reduced levels of [Fe−S] cluster/haem-containing subunits of individual mitochondrial respiratory complexes, NDUFB8 (CI), SDHB (CII), UQCRC2 (CIII), and MTCO2 (CIV), in both SELENOK-knockdown/knockout neurons and N2a cells. The above results indicate that SELENOK deficiency impairs iron−sulfur [Fe−S] cluster/haem biogenesis.

Research has found that iron sulfur clusters are closely related to iron homeostasis, For instance, the deficiency of NADH dehydrogenase [ubiquinone] iron−sulfur protein 4 (NDUFS4), a subunit of Complex I, may lead to iron perturbations.[49] In humans, the majority of iron (over 75%) is directly used for the synthesis of haem or Fe−S cluster cofactors.[16] Hence, the concentration of iron is significant in the assembly of Fe−S clusters. TfR-1 binds to and internalizes ferric ($Fe^{3+}$)-loaded transferrin (Tf).[50] Under conditions of low iron, iron regulatory protein (IRP1/2) binds to the conserved hairpin structure known as the IRE located in the 3′-UTR of TfR-1 mRNA, selectively stabilizing the mRNA and ensuring appropriate TfR-1 cell surface expression and the uptake of TfR-1-bound iron.[50−52] Conversely, under conditions of excess iron, IRP-1 becomes cytosolic aconitase, which catalyzes the conversion of citrate into isocitrate, while IRP-2 undergoes degradation by proteasomes; consequently, these two proteins no longer connect with IREs, resulting in diminished TfR-1 expression, which leads to less expression on the cell surface and a decrease in the uptake of iron bound to TfR-1,.[53−55] Our findings revealed a significant decrease in the Fe content in the SELENOK$^{-/-}$ cells and mice. Additionally, both the mitochondrial and cytoplasmic iron contents were significantly reduced. The significant upregulation of IREB2, Tf, and TfR-1 and the downregulation of FTH1 also suggested an iron starvation response and iron−sulfur cluster deficiency in SELENOK-knockout or SELENOK-knockdown mice and neurons.[56] These findings provide further confirmation that SELENOK deficiency leads to reduced intracellular iron content and impairs iron−sulfur [Fe−S] cluster/haem biogenesis.

Iron transport primarily occurs through the endocytosis of TfR-1, and the membrane localization of TfR-1 necessitates posttranslational palmitoylation.[32] SELENOK acts as a chaperone for DHHC6, participating in various protein palmitoylation modification processes.[41] Consequently, a significant reduction in TfR-1 palmitoylation and decreased expression on the cell membrane were observed both in vitro and in vivo, indicating that SELENOK knockout affects TfR-1 palmitoylation and subsequently alters the distribution of TfR-1. Further investigation of the function of TfR-1 through the Tf transport rate revealed a significant reduction in the Tf transport rate in SELENOK knockout/knockdown cells. Artesunate, an artemisinin derivative, is known to enhance the palmitoylation of TfR-1,.[57] Both artesunate treatment and overexpression of SELENOK significantly enhanced TfR-1 palmitoylation and cell membrane expression in SELENOK$^{-/-}$ N2a cells. Moreover, this led to a notable increase in the Tf transport rate and $Fe^{2+}$ content. These findings confirm that SELENOK regulates the palmitoylation of TfR-1 via DHHC6 and mediates its expression on the neuronal cytoplasmic membrane, thereby influencing iron transport and causing mitochondrial dysfunction.

Previous studies have demonstrated that knockout of the SELENOK gene causes a marked drop in memory and an increase in anxiety in mice.[30] However, supplementation with iron or restoration of SELENOK expression reverses the decline in learning and memory abilities and alleviates the increase in anxiety caused by SELENOK gene knockout. Furthermore, iron supplementation and restoration of SELENOK expression significantly increased the iron content and restored the ATP content. These results confirm that SELENOK knockout/knockdown leads to a reduction in iron content by decreasing the level of TfR-1 palmitoylation, thereby impairing the assembly of mitochondrial iron−sulfur clusters and compromising mitochondrial function. This is a new mechanism, distinct from antioxidation, that directly regulates iron homeostasis.

Iron is crucial for brain activities like neuron development, electron transport and respiration.[58] The absence of sufficient iron impairs gene expression and energy metabolism in neurons developing in the hippocampus.[59] Children suffering from iron deficiency exhibited a significant reduction in cognitive and motor abilities compared to their healthy counterparts.[60] Low Se status has been linked to heightened mortality risks and cognitive decline.[61,62] Studies have demonstrated that Se deficiency leads to cognitive problems, including immature neurodevelopment, reduced long-term potentiation (LTP) and learning abilities in experimental animals.[63,64] Besides, supplementing with Se enhanced the cognitive abilities and synaptic plasticity in mice.[65,66] So adequate supplementation of iron and selenium is beneficial for cognitive function in the elderly.[67] However, while Se supplementation inhibits ferroptosis by upregulating the expression of selenoproteins such as GPX4, TXNRD1, and SELENOK,[27,68] there is limited research on the direct interaction between selenium/selenoproteins and iron. Our research uncovers that SELENOK maintains normal mitochondrial function and protects neurons by regulating iron homeostasis, with its expression level being modulated by dietary selenium. Therefore, this study presents innovative ideas and solid evidence regarding the correlation between Se and iron metabolism.

In summary, this study provides compelling evidence that SELENOK modulates the palmitoylation of TfR-1, resulting in decreased intracellular iron levels and impaired iron−sulfur cluster assembly, and ultimately leading to mitochondrial dysfunction and reduced cell viability. Our findings elucidate a novel mechanism by which SELENOK regulates iron homeostasis through its involvement in TfR-1 palmitoylation, and provide new insights into the neuroprotective effects of


https://doi.org/10.1021/acs.jafc.4c08266
J. Agric. Food Chem. 2025, 73, 12233−12246

selenium and selenoproteins in the treatment of neurodegenerative diseases.

## ■ ASSOCIATED CONTENT

### Supporting Information

The Supporting Information is available free of charge at https://pubs.acs.org/doi/10.1021/acs.jafc.4c08266.

SELENOK expression level detection in vitro and in vivo (Figure S1), SELENOK deficiency reduces iron−sulfur cluster protein expression in SELENOK$^{-/-}$ mice (Figure S2), iron deficiency reduces iron−sulfur cluster protein expression in vitro (Figure S3), SELENOK knockdown reduces iron content and impairs mitochondrial function in primary neurons (Figure S4), restoring the expression of SELENOK/artesunate treatment enhances the iron content in neurons (Figure S5) (PDF)

## ■ AUTHOR INFORMATION


### Corresponding Authors

**Zhong-Hao Zhang** − *Shenzhen Key Laboratory of Marine Bioresources and Ecology, Brain Disease and Big Data Research Institute, College of Life Sciences and Oceanography, Shenzhen University, Shenzhen 518060, China; Shenzhen-Hong Kong Institute of Brain Science-Shenzhen Fundamental Research Institutions, Shenzhen 518060, China;* orcid.org/0000-0001-5640-5670; Email: zzh@szu.edu.cn

**Guo-Li Song** − *Shenzhen Key Laboratory of Marine Bioresources and Ecology, Brain Disease and Big Data Research Institute, College of Life Sciences and Oceanography, Shenzhen University, Shenzhen 518060, China; Shenzhen-Hong Kong Institute of Brain Science-Shenzhen Fundamental Research Institutions, Shenzhen 518060, China;* orcid.org/0000-0003-0521-668X; Email: lilys@szu.edu.cn

### Authors

**Shi-Zheng Jia** − *Shenzhen Key Laboratory of Marine Bioresources and Ecology, Brain Disease and Big Data Research Institute, College of Life Sciences and Oceanography, Shenzhen University, Shenzhen 518060, China; Guangdong Key Laboratory for Biomedical Measurements and Ultrasound Imaging, School of Biomedical Engineering, Shenzhen University Health Science Center, Shenzhen 518060, China*

**Yu Li** − *Shenzhen Key Laboratory of Marine Bioresources and Ecology, Brain Disease and Big Data Research Institute, College of Life Sciences and Oceanography, Shenzhen University, Shenzhen 518060, China*

**Xin-Wen Xu** − *Shenzhen Key Laboratory of Marine Bioresources and Ecology, Brain Disease and Big Data Research Institute, College of Life Sciences and Oceanography, Shenzhen University, Shenzhen 518060, China*

**Yan-Ping Huang** − *Shenzhen Key Laboratory of Marine Bioresources and Ecology, Brain Disease and Big Data Research Institute, College of Life Sciences and Oceanography, Shenzhen University, Shenzhen 518060, China*

**Xiao-Yi Deng** − *Shenzhen Key Laboratory of Marine Bioresources and Ecology, Brain Disease and Big Data Research Institute, College of Life Sciences and Oceanography, Shenzhen University, Shenzhen 518060, China*

Complete contact information is available at: https://pubs.acs.org/10.1021/acs.jafc.4c08266


### Notes

The authors declare no competing financial interest.

## ■ ACKNOWLEDGMENTS

This research was funded by the National Natural Sciences Foundation of China [grant number 32171223]; Shenzhen University 2035 Initiative [grant number 2023C002], and also thank the Instrumental Analysis Center of Shenzhen University (Shenzhen, China) for their assistance in our experiments.

## ■ REFERENCES


(1) Borcherding, N.; Brestoff, J. R. The power and potential of mitochondria transfer. *Nature* **2023**, *623* (7986), 283−291.

(2) Ghifari, A. S.; Saha, S.; Murcha, M. W. The biogenesis and regulation of the plant oxidative phosphorylation system. *Plant Physiol.* **2023**, *192* (2), 728−747.

(3) Koopman, W. J.; Nijtmans, L. G.; Dieteren, C. E.; Roestenberg, P.; Valsecchi, F.; Smeitink, J. A.; Willems, P. H. Mammalian mitochondrial complex I: biogenesis, regulation, and reactive oxygen species generation. *Antioxid. Redox Signaling* **2010**, *12* (12), 1431−1470.

(4) Cecchini, G. Function and structure of complex II of the respiratory chain. *Ann. Rev. Biochem.* **2003**, *72* (1), 77−109.

(5) Di Donato, S. Disorders related to mitochondrial membranes: pathology of the respiratory chain and neurodegeneration. *J. Inherited Metab. Dis.* **2000**, *23* (3), 247−263.

(6) Hernansanz-Agustín, P.; Enríquez, J. A. Sodium in Mitochondrial Redox Signaling. *Antioxid. Redox Signaling* **2022**, *37* (4−6), 290−300.

(7) Nakano, A.; Kishikawa, J.-i.; Mitsuoka, K.; Yokoyama, K. Mechanism of ATP hydrolysis dependent rotation of bacterial ATP synthase. *Nat. Commun.* **2023**, *14* (1), 4090.

(8) Klemmensen, M. M.; Borrowman, S. H.; Pearce, C.; Pyles, B.; Chandra, B. Mitochondrial dysfunction in neurodegenerative disorders. *Neurotherapeutics* **2024**, *21*, No. e00292.

(9) Klecker, T.; Westermann, B. Pathways shaping the mitochondrial inner membrane. *Open Biol.* **2021**, *11* (12), 210238.

(10) Dale, N.; Butler, J.; Dospinescu, V.-M.; Nijjar, S. Channel-mediated ATP release in the nervous system. *Neuropharmacology* **2023**, *227*, 109435.

(11) Read, A. D.; Bentley, R. E.; Archer, S. L.; Dunham-Snary, K. J. Mitochondrial iron−sulfur clusters: Structure, function, and an emerging role in vascular biology. *Redox Biol.* **2021**, *47*, 102164.

(12) Jain, I. H.; Calvo, S. E.; Markhard, A. L.; Skinner, O. S.; To, T.-L.; Ast, T.; Mootha, V. K. Genetic screen for cell fitness in high or low oxygen highlights mitochondrial and lipid metabolism. *Cell* **2020**, *181* (3), 716−727e11.

(13) Maio, N.; Ghezzi, D.; Verrigni, D.; Rizza, T.; Bertini, E.; Martinelli, D.; Zeviani, M.; Singh, A.; Carrozzo, R.; Rouault, T. A. Disease-causing SDHAF1 mutations impair transfer of Fe-S clusters to SDHB. *Cell Metab.* **2016**, *23* (2), 292−302.

(14) Purhonen, J.; Grigorjev, V.; Ekiert, R.; Aho, N.; Rajendran, J.; Pietras, R.; Truvé, K.; Wikström, M.; Sharma, V.; Osyczka, A.; et al. A spontaneous mitonuclear epistasis converging on Rieske Fe-S protein exacerbates complex III deficiency in mice. *Nat. Commun.* **2020**, *11* (1), 322.

(15) Nyvltova, E.; Dietz, J.; Seravalli, J.; Khalimonchuk, O.; Barrientos, A. Coordination of metal center biogenesis in human cytochrome c oxidase. *Nat. Commun.* **2022**, *13* (1), 3615−M.

(16) Barupala, D. P.; Dzul, S. P.; Riggs-Gelasco, P. J.; Stemmler, T. L. Synthesis, delivery and regulation of eukaryotic heme and Fe−S cluster cofactors. *Arch. Biochem. Biophys.* **2016**, *592*, 60−75.

(17) Yanatori, I.; Richardson, D. R.; Dhekne, H. S.; Toyokuni, S.; Kishi, F. CD63 is regulated by iron via the IRE-IRP system and is

important for ferritin secretion by extracellular vesicles. *Blood* **2021**, *138* (16), 1490−1503.
(18) Caltagirone, A.; Weiss, G.; Pantopoulos, K. Modulation of cellular iron metabolism by hydrogen peroxide: effects of H2O2 on the expression and function of iron-responsive element-containing mRNAs in B6 fibroblasts. *J. Biol. Chem.* **2001**, *276* (23), 19738−19745.
(19) Rouault, T. A. The role of iron regulatory proteins in mammalian iron homeostasis and disease. *Nat. Chem. Biol.* **2006**, *2* (8), 406−414.
(20) Kawabata, H. Transferrin and transferrin receptors update. *Free Radical Biol. Med.* **2019**, *133*, 46−54.
(21) Cheng, Y.; Zak, O.; Aisen, P.; Harrison, S. C.; Walz, T. Structure of the human transferrin receptor-transferrin complex. *Cell* **2004**, *116* (4), 565−576.
(22) Soares de Oliveira, A. R.; Jayanne Clímaco Cruz, K.; Beatriz Silva Morais, J.; Rocha Dos Santos, L.; Rodrigues de Sousa Melo, S.; Fontenelle, L. C.; Santos de Sousa, G.; Costa Maia, C. S.; Oliveira Duarte de Araújo, C.; Leal Mendes, I.; et al. Selenium status and oxidative stress in obese: Influence of adiposity. *Eur. J. Clin. Invest.* **2021**, *51* (9), No. e13538.
(23) Culhuac, E. B.; Elghandour, M. M.; Adegbeye, M. J.; Barbabosa-Pliego, A.; Salem, A. Z. Influence of dietary selenium on the oxidative stress in horses. *Biol. Trace Elem. Res.* **2023**, *201* (4), 1695−1703.
(24) Nakayama, A.; Hill, K. E.; Austin, L. M.; Motley, A. K.; Burk, R. F. All regions of mouse brain are dependent on selenoprotein P for maintenance of selenium. *J. Nutr.* **2007**, *137* (3), 690−693.
(25) Chen, J.; Berry, M. J. Selenium and selenoproteins in the brain and brain diseases. *J. Neurochem.* **2003**, *86* (1), 1−12.
(26) Chen, C.; Chen, Y.; Zhang, Z.-H.; Jia, S.-Z.; Chen, Y.-B.; Huang, S.-L.; Xu, X.-W.; Song, G.-L. Selenomethionine improves mitochondrial function by upregulating mitochondrial selenoprotein in a model of Alzheimer's disease. *Front. Aging Neurosci.* **2021**, *13*, 750921.
(27) Alim, I.; Caulfield, J. T.; Chen, Y.; Swarup, V.; Geschwind, D. H.; Ivanova, E.; Seravalli, J.; Ai, Y.; Sansing, L. H.; Ste Marie, E. J.; et al. Selenium drives a transcriptional adaptive program to block ferroptosis and treat stroke. *Cell* **2019**, *177* (5), 1262−1279.e25.
(28) Verma, S.; Hoffmann, F. W.; Kumar, M.; Huang, Z.; Roe, K.; Nguyen-Wu, E.; Hashimoto, A. S.; Hoffmann, P. R. Selenoprotein K knockout mice exhibit deficient calcium flux in immune cells and impaired immune responses. *J. Immunol.* **2011**, *186* (4), 2127−2137.
(29) Zhang, Y.; Zhou, Y.; Schweizer, U.; Savaskan, N. E.; Hua, D.; Kipnis, J.; Hatfield, D. L.; Gladyshev, V. N. Comparative analysis of selenocysteine machinery and selenoproteome gene expression in mouse brain identifies neurons as key functional sites of selenium in mammals. *J. Biol. Chem.* **2008**, *283* (4), 2427−2438.
(30) Jia, S.-Z.; Xu, X.-W.; Zhang, Z.-H.; Chen, C.; Chen, Y.-B.; Huang, S.-L.; Liu, Q.; Hoffmann, P. R.; Song, G.-L. Selenoprotein K deficiency-induced apoptosis: A role for calpain and the ERS pathway. *Redox Biol.* **2021**, *47*, 102154.
(31) Fredericks, G. J.; Hoffmann, F. W.; Rose, A. H.; Osterheld, H. J.; Hess, F. M.; Mercier, F.; Hoffmann, P. R. Stable expression and function of the inositol 1, 4, 5-triphosphate receptor requires palmitoylation by a DHHC6/selenoprotein K complex. *Proc. Natl. Acad. Sci. U.S.A.* **2014**, *111* (46), 16478−16483.
(32) Drecourt, A.; Babdor, J.; Dussiot, M.; Petit, F.; Goudin, N.; Garfa-Traoré, M.; Habarou, F.; Bole-Feysot, C.; Nitschké, P.; Ottolenghi, C.; et al. Impaired transferrin receptor palmitoylation and recycling in neurodegeneration with brain iron accumulation. *Am. J. Hum. Genet.* **2018**, *102* (2), 266−277.
(33) Petit, F.; Drecourt, A.; Dussiot, M.; Zangarelli, C.; Hermine, O.; Munnich, A.; Rötig, A. Defective palmitoylation of transferrin receptor triggers iron overload in Friedreich ataxia fibroblasts. *Blood* **2021**, *137* (15), 2090−2102.
(34) Zhang, Z.-H.; Wu, Q.-Y.; Zheng, R.; Chen, C.; Chen, Y.; Liu, Q.; Hoffmann, P. R.; Ni, J.-Z.; Song, G.-L. Selenomethionine mitigates cognitive decline by targeting both tau hyperphosphorylation and autophagic clearance in an Alzheimer's disease mouse model. *J. Neurosci.* **2017**, *37* (9), 2449−2462.
(35) Ouyang, P.; Cai, Z.; Peng, J.; Lin, S.; Chen, X.; Chen, C.; Feng, Z.; Wang, L.; Song, G.; Zhang, Z. SELENOK-dependent CD36 palmitoylation regulates microglial functions and A$\beta$ phagocytosis. *Redox Biol.* **2024**, *70*, 103064.
(36) Wan, J.; Roth, A. F.; Bailey, A. O.; Davis, N. G. Palmitoylated proteins: purification and identification. *Nat. Protoc.* **2007**, *2* (7), 1573−1584.
(37) Huang, L. H.; Lane, D. J. R.; Richardson, D. R. Mitochondrial mayhem: the mitochondrion as a modulator of iron metabolism and its role in disease. *Antioxid. Redox Signaling* **2011**, *15* (12), 3003−3019.
(38) Richardson, D. R.; Lane, R. J. R.; Becker, R. M.; Huang, L. H.; Whitnall, M.; Rahmanto, Y. S.; Sheftel, R. D.; Ponka, R. Mitochondrial iron trafficking and the integration of iron metabolism between the mitochondrion and cytosol. *Proc. Natl. Acad. Sci. U.S.A.* **2010**, *107* (24), 10775−10782.
(39) Sakajiri, T.; Yamamura, T.; Kikuchi, T.; Yajima, H. Computational structure models of apo and diferric transferrin−transferrin receptor complexes. *Protein J.* **2009**, *28*, 407−414.
(40) Chen, G.-Q.; Benthani, F. A.; Wu, J.; Liang, D.; Bian, Z.-X.; Jiang, X. Artemisinin compounds sensitize cancer cells to ferroptosis by regulating iron homeostasis. *Cell Death Differ.* **2020**, *27* (1), 242−254.
(41) Fredericks, G. J.; Hoffmann, F. W.; Hondal, R. J.; Rozovsky, S.; Urschitz, J.; Hoffmann, P. R. Selenoprotein K increases efficiency of DHHC6 catalyzed protein palmitoylation by stabilizing the acyl-DHHC6 intermediate. *Antioxidants* **2018**, *7* (1), 4.
(42) Staneviciene, I.; Sulinskiene, J.; Sadauskiene, I.; Liekis, A.; Ruzgaite, A.; Naginiene, R.; Baranauskiene, D.; Simakauskiene, V.; Krusnauskas, R.; Viezeliene, D. Effect of selenium on the iron homeostasis and oxidative damage in brain and liver of mice. *Antioxidants* **2022**, *11* (7), 1216.
(43) Christensen, M. J.; Olsen, C. A.; Hansen, D. V.; Ballif, B. C. Selenium regulates expression in rat liver of genes for proteins involved in iron metabolism. *Biol. Trace Elem. Res.* **2000**, *74*, 55−70.
(44) Yang, M.; Tsui, M. G.; Tsang, J. K. W.; Goit, R. K.; Yao, K.-M.; So, K.-F.; Lam, W.-C.; Lo, A. C. Y. Involvement of FSP1-CoQ10-NADH and GSH-GPx-4 pathways in retinal pigment epithelium ferroptosis. *Cell Death Dis.* **2022**, *13* (5), 468.
(45) Ward, R. J.; Zucca, F. A.; Duyn, J. H.; Crichton, R. R.; Zecca, L. The role of iron in brain ageing and neurodegenerative disorders. *Lancet Neurol.* **2014**, *13* (10), 1045−1060.
(46) Baron, M.; Kudin, A.; Kunz, W. Mitochondrial dysfunction in neurodegenerative disorders. *Biochem. Soc. Trans.* **2007**, *35* (5), 1228−1231.
(47) Jia, S.; Xu, X.; Zhang, Z.; Chen, C.; Chen, Y.; Huang, S.; Liu, Q.; Hoffmann, P.; Song, G. Selenoprotein K deficiency-induced apoptosis: A role for calpain and the ERS pathway. *Redox Biol.* **2021**, *47*, 102154.
(48) Meyer, E. H.; Welchen, E.; Carrie, C. Assembly of the complexes of the oxidative phosphorylation system in land plant mitochondria. *Annu. Rev. Plant Biol.* **2019**, *70*, 23−50.
(49) Kelly, C.; Couch, R. K.; Ha, V. T.; Bodart, C. M.; Wu, J.; Huff, S.; Herrel, N. T.; Kim, H. D.; Zimmermann, A. O.; Shattuck, J.; et al. Iron status influences mitochondrial disease progression in Complex I-deficient mice. *Elife* **2023**, *12*, No. e75825.
(50) Aisen, P. Transferrin receptor 1. *Int. J. Biochem. Cell Biol.* **2004**, *36* (11), 2137−2143.
(51) Pantopoulos, K. Iron metabolism and the IRE/IRP regulatory system: an update. *Ann. N.Y. Acad. Sci.* **2004**, *1012* (1), 1−13.
(52) Charlebois, E.; Fillebeen, C.; Katsarou, A.; Rabinovich, A.; Wisniewski, K.; Venkataramani, V.; Michalke, B.; Velentza, A.; Pantopoulos, K. A crosstalk between hepcidin and IRE/IRP pathways controls ferroportin expression and determines serum iron levels in mice. *Elife* **2022**, *11*, No. e81332.
(53) Haile, D. J.; Rouault, T. A.; Harford, J. B.; Kennedy, M. C.; Blondin, G. A.; Beinert, H.; Klausner, R. D. Cellular regulation of the

iron-responsive element binding protein: disassembly of the cubane iron-sulfur cluster results in high-affinity RNA binding. *Proc. Natl. Acad. Sci. U.S.A.* **1992**, *89* (24), 11735−11739.
(54) Guo, B.; Phillips, J. D.; Yu, Y.; Leibold, E. A. Iron Regulates the Intracellular Degradation of Iron Regulatory Protein 2 by the Proteasome (*). *J. Biol. Chem.* **1995**, *270* (37), 21645−21651.
(55) Müllner, E. W.; Neupert, B.; Kühn, L. C. A specific mRNA binding factor regulates the iron-dependent stability of cytoplasmic transferrin receptor mRNA. *Cell* **1989**, *58* (2), 373−382.
(56) Terzi, E. M.; Sviderskiy, V. O.; Alvarez, S. W.; Whiten, G. C.; Possemato, R. Iron-sulfur cluster deficiency can be sensed by IRP2 and regulates iron homeostasis and sensitivity to ferroptosis independent of IRP1 and FBXL5. *Sci. Adv.* **2021**, *7* (22), No. eabg4302.
(57) Petit, F.; Drecourt, A.; Dussiot, M.; Zangarelli, C.; Hermine, O.; Munnich, A.; Rötig, A. Defective palmitoylation of transferrin receptor triggers iron overload in Friedreich ataxia fibroblasts. *Blood* **2021**, *137* (15), 2090−2102.
(58) Rouault, T. A. Iron metabolism in the CNS: implications for neurodegenerative diseases. *Nat. Rev. Neurosci.* **2013**, *14* (8), 551−564.
(59) Bastian, T. W.; von Hohenberg, W. C.; Mickelson, D. J.; Lanier, L. M.; Georgieff, M. K. Iron deficiency impairs developing hippocampal neuron gene expression, energy metabolism, and dendrite complexity. *Dev. Neurosci.* **2016**, *38* (4), 264−276.
(60) Otero, G. A.; Pliego-Rivero, F. B.; Porcayo-Mercado, R.; Mendieta-Alcántara, G. Working memory impairment and recovery in iron deficient children. *Clin. Neurophysiol.* **2008**, *119* (8), 1739−1746.
(61) Rayman, M. P. Selenium and human health. *Lancet* **2012**, *379* (9822), 1256−1268.
(62) Schomburg, L. Selenium, selenoproteins and the thyroid gland: interactions in health and disease. *Nat. Rev. Endocrinol.* **2012**, *8* (3), 160−171.
(63) Babür, E.; Tan, B.; Yousef, M.; Cinbaş, S.; Süer, C.; Dursun, N. Deficiency but not supplementation of selenium impairs the hippocampal long-term potentiation and hippocampus-dependent learning. *Biol. Trace Elem. Res.* **2019**, *192*, 252−262.
(64) Zhang, S.-Q. Selenium and cognitive function. *Metab. Brain Dis.* **2023**, *38* (1), 221−222.
(65) Zhang, X.; He, H.; Xiang, J.; Li, B.; Zhao, M.; Hou, T. Selenium-containing soybean antioxidant peptides: Preparation and comprehensive comparison of different selenium supplements. *Food Chem.* **2021**, *358*, 129888.
(66) Zhang, Z.-H.; Chen, C.; Jia, S.-Z.; Cao, X.-C.; Liu, M.; Tian, J.; Hoffmann, P. R.; Xu, H.-X.; Ni, J.-Z.; Song, G.-L. Selenium Restores Synaptic Deficits by Modulating NMDA Receptors and Selenoprotein K in an Alzheimer's Disease Model. *Antioxid. Redox Signaling* **2021**, *35* (11), 863−884.
(67) Lu, K.; Liu, T.; Wu, X.; Zhong, J.; Ou, Z.; Wu, W. Association between serum iron, blood lead, cadmium, mercury, selenium, manganese and low cognitive performance in old adults from National Health and Nutrition Examination Survey (NHANES): a cross-sectional study. *Br. J. Nutr.* **2023**, *130* (10), 1743−1753.
(68) Yang, W. S.; SriRamaratnam, R.; Welsch, M. E.; Shimada, K.; Skouta, R.; Viswanathan, V. S.; Cheah, J. H.; Clemons, P. A.; Shamji, A. F.; Clish, C. B.; et al. Regulation of ferroptotic cancer cell death by GPX4. *Cell* **2014**, *156* (1−2), 317−331.


https://doi.org/10.1021/acs.jafc.4c08266
*J. Agric. Food Chem.* 2025, 73, 12233−12246